High Level Trigger Studies for the ATLAS Detector

Efstathios (Stathis) Stefanidis

First Year Transfer Report

University College London
Department of Physics and Astronomy
High Energy Physics Group

4th June 2004

Abstract

An overview of the studies that have been done, during my first year, on the High Level Trigger for the ATLAS Detector is presented. The work consists of the performance studies on the IDScan tracking algorithm for the Level-2, the e/γ vertical slice for triggering physics events in which electrons and photons are involved and finally, the very preliminary effort for optimizing the size of the Region of Interest, which plays a crusial role, as explained in the main text. My future plans for the further performance and physics studies are given at the end of this report.

Preface

During the last decades, the effort for understanding the origin and the structure of our Universe has been focused on the particle accelarators, which lead reseach towards higher energies, probing more and more the hidden areas of particle physics. The discovery of the top quark at Tevatron is a recent example for the potentialities of the new accelarating machines. Into this new era, the Large Handron Collider (LHC) at CERN will offer the highest energy ever achived, thus extending our knowledge for the world around us. LHC will accelarate two proton beams with energy of 7 TeV each and the first collisions are expected to start at the middle of 2007.

The electroweak theory proved to be correct with the prediction and -finally- the discovery of the W, Z vector bosons at the SPS accelarator. These vector bosons get their mass by introducing a scalar doublet, which breaks the symmetry between the four vector bosons of the electroweak theory (W^-, W^+, Z^o, γ). By assigning to each fermion particle a coupling (which is analogous to its mass) with this scalar field, we manage to explain and interpret the masses of all known particles as the interaction of the particles with this scalar field.

The scalar field, which is called **Higgs Field**, predicts the existence of a carrier, the **Higgs boson**, the discovery of which will give the missing piece to the theory of **Standard Model**. Further theories, such as **SuperSymmetry**, predict some extra Higgs particles. Because of the high energy gained by the protons at the LHC and due to the specific construction features of the ATLAS detector, all these theories will be tested and -probably- verified. Either success or failure of these theories, will give science a big opportunity for making a step further towards Ithaca.

The first chapter of this report refers to the ATLAS Detector, in general. The second chapter describes the Triggering System of the Detector and, particularly, the High Level Trigger. This is followed by the performance studies I have done on the IDScan and on the e/gamma Selection Algorithms. The final chapter gives my future plans, including the physics which I shall study.

Now that I have reached the end of my first year of my PhD studies, I can't avoid thanking, first of all, my supervisor, Dr. N. Konstantinidis, for his continuous support and encouragement. I also thank all the members of the group who welcomed me and helped me feel inside the group as home.

Contents

List of Figures

Chapter 1

LHC - ATLAS.

1.1 The design of the LHC collider.

The Large Hadron Collider (LHC - [1]) is being installed at the already existent LEP tunnel. LHC will provide proton-proton collisions and heavy-ion collisions as well (for example Pb-Pb). In the case of pp collisions, the center of mass energy will be 14 TeV (7 times higher that the Tevatron machine at Fermilab), while the luminosity will reach the value of $10^{34} cm^{-2} s^{-1}$ (100 times larger compared to LEP and Tevatron). Under these conditions, there will be the space for detection and study of particles with mass up to 5 TeV approximately.

The beam collisions will occur each 25 ns. From the value of the cross section for the inelastic pp collision ($\sigma_{inel}^{pp} = 80\, mb$) and with the luminosity mentioned earlier, one can easily find[1] that there will be approximately 10^9 interactions per second.

Two phases are foreseen during the LHC operation: at the beginning, the luminosity will be $2 \times 10^{33} cm^{-2} s^{-1}$ (the so-called **low luminosity phase**) and will reach the design luminosity of $10^{34} cm^{-2} s^{-1}$ (**high luminosity phase**).

1.2 The design of the ATLAS Detector.

The ATLAS Detector (**A** **T**oroidal **L**HC **A**pparatu**S** - [2]) is a general-purpose detector. Fig. 1.1 shows the overall picture of the detector. It mainly consists of three parts: the Inner Detector, which is inside a solenoid magnetic field, the Calorimeter (Electromagnetic -EM- and Hadronic -HAD) and the Muon Spectrometer, which is inside a toroid magnetic field.

The **Inner Detector** uses two different technologies: near the interaction point there are Semiconductor tracking detectors, using silicon microstrip (SCT) and Pixel technologies. They provide position information with high accuracy. Outermost, there is the Transition Radiation Tracker (TRT), which is designed for particle identification. Both parts are ment to cope with the high interaction rates of LHC.

The **Calorimeter** is made up of different layers. The electromagnetic calorimeter comes first. It is a sampling calorimeter with liguid argon (LAr) between the lead plates. The hadronic calorimeter uses scintillators with Fe and Cu Tiles as absorbers. The calorimeter is designed to cover regions even very close to the beam pipe, where no other detector element exists.

Finally, the **Muon Spectrometer** consists of the drift chambers, placed into three layers, covering the barrel and the end-cap region, as well. The chambers are into a toroid magnetic field, which bends the tracks of the charged muons and is designed for independent performance and measurments of the position and momentum.

Briefly, the main performance requirements are:

1. Measurement of leptons over the p_T range from few GeV up to a few TeV. Soft leptons are produced in decays of the B-hadrons, while decays of heavy particles will give high energetic leptons.

2. Hermetic calorimetry for reliable measurments of the missing transverse energy. This is needed not only to detect neutrinos, but to detect the forward jets produced in association with a heavy Higgs boson.

[1] $N = L \cdot \sigma_{inel}^{pp} = 10^{34} cm^{-2} s^{-1} \cdot 80 \cdot 10^{-3} \cdot 10^{-24} cm^2 = 8 \cdot 10^8\ interactions/sec$

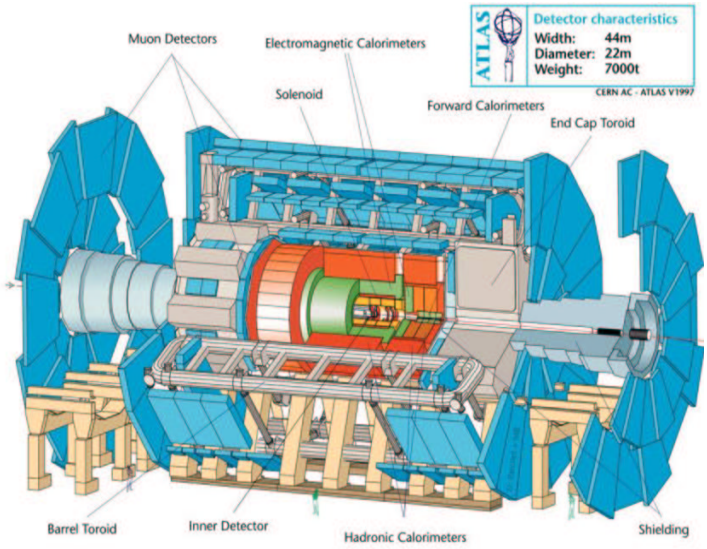

Figure 1.1: *Overall view of the ATLAS Detector. The detector is 44 m long and has 11 m radius.*

Table 1.1: *The main features of the ATLAS detector. From [3].*

System	**Features**
Magnet(s)	Air-core toroids + solenoid in inner cavity Calorimeters outside field 4 magnets
Inner Detector	Si layers (pixels and strips) TRT $\rightarrow$ particle identification B = 2 T $\sigma/p_T \sim 5 \times 10^{-4} p_T(GeV) \bigoplus 0.01$
EM calorimeter	Lead-liquid argon $\sigma/E \sim 10\%/\sqrt{E(GeV)}$ Longitudinal segmentation
HAD calorimeter	Fe+scintillator + Cu-liquid argon $> 10\lambda$ $\sigma/E \sim 50\%/\sqrt{E(GeV)} \bigoplus 0.03$
Muon spectrometer	Air $\sigma/p_T \sim 7\%$ at 1 TeV achieved by spectrometer alone

3. Very good mass resolution ($\sim$ 1%) for particles of masses up to a few hundreds GeV, which decay into photons or leptons. In that case, the irreducible background has larger cross section than the signal, so a very good mass resolution is needed to allow the observation of a clear resonance above the continuum background spectrum.

4. Excellent electron/jet and photon/jet separation.

5. Very selective and -at the same time- efficient trigger. In order to reach the storage space, the interaction rate of 10^9 events/s must be reduced to 100 events/s and the latency of the whole trigger system should be around 2 ms.

Finally, Table 1.1 summarizes the main features of the detector.

Chapter 2

The ATLAS Trigger and Data Acquisition System.

2.1 Overview.

As mentioned in Chapter 1, the bunch crossing rate at LHC is one every 25 ns (40 MHz), giving about 23 proton-proton interactions per bunch crossing during the high luminosity phase. The triggering system of the detector has to reduce this rate down approximately to 100 Hz, under the resistrictions of the computing power and storage capabilities. This has to been done with a very efficient, unbiased and robust event selection, rejecting the background events and storing the interesting candidate ones.

The ATLAS Trigger System [4] is designed in three-levels, which is a typical architecture for the HEP Detectors. Fig. 2.1 gives a schematic overview of the Trigger and DAQ system, while Fig. 2.2 gives the corresponding latencies for each level.

The first level trigger (**LVL1**) has to reduce the 40 MHz rate of the bunch crossing to 75 kHz, within a period of time less than 2.5 μs. It is a hardware trigger and uses the reduced granularity information from the calorimeter and the muon system to reject the un-interesting events and to identify the **Regions of Interest** (**RoI** -see section 2.2.1). In this stage, the detector data are held in the pipeline memories and events which are accepted by LVL1 are then transferred to **Read-Out Buffers (ROB)**, where they are held pending the LVL2.

LVL2 reduces the event rate further to 2 kHz, with an available decision time of about 10 ms. Now, the whole information of all detector elements (full granularity information from calorimeters and precision muon chambers and the inner detector) is avalaible and can be retrievied from the ROB. The RoIs, seeded by LVL1, play a crusial role here, because they define the regions, where the data will be retrievied from. Thus, the amount of requested data ends up to be only a few percent of the full event. It is important here to have specialised trigger algorithms (e.g IDScan - see section 2.2.4), which can reconstruct the tracks fast and, by applying specific cuts, reject or accept the event. In the case of an accepted event, the data fragments for all ROB are sent to Event Builder, which builds the whole event and passes it to the last level.

Finally, the Event Filter (**EF**) applies more sophisticated reconstruction algorithms and uses mole detailed calibration and alignment data. The available time is approximately 2 s and the the event rate becomes about 200 Hz.

Together, LVL2 and EF are known as the **High Level Trigger (HLT)** and they have a large part of their infrasturcture in common.

2.2 High Level Trigger.

2.2.1 Region of Interest mechanism.

The Region of Interest (RoI) is a very significant and foundamental mechanism, from which the HLT starts. As mentioned before, the LVL1 trigger is based on the "rough" information coming from the muon spectrometer and the calorimeter. The RoI is the geographical object which is formed by the combined signatures of these two systems and defines the area where HLT will search at (Fig. 2.3). After a RoI has been formed by LVL1, it is passed to LVL2, it is quickly decoded to give all the ROB inside it and finally the data from one detector at a time which is into these ROB, are requested sequentially. By that way, **only the data**

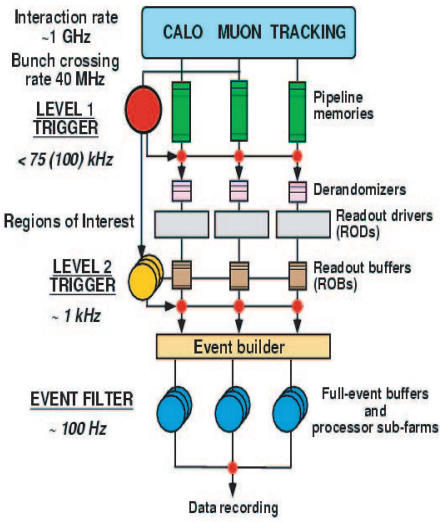

Figure 2.1: *Overview of the ATLAS Trigger/DAQ System.*

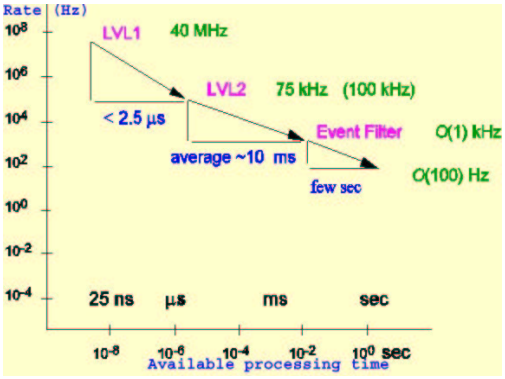

Figure 2.2: *Event rates and available decision time for each trigger level.*

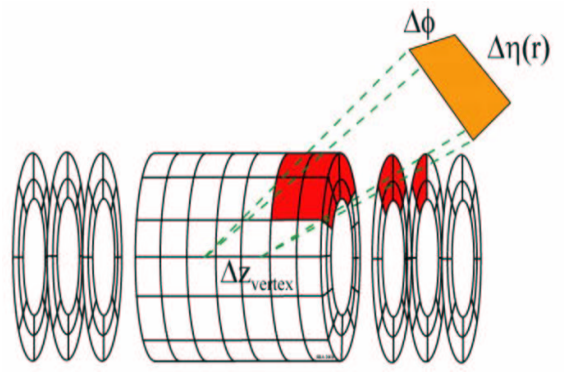

Figure 2.3: *The geometry of the Regions of Interest (RoIs).*

Table 2.1: *Example of trigger menus and the corresponding physics signatures. The required values for p_T and E_T are given for the low luminosity phase.*

Objects	Selection Signatures	Examples of physics coverage
Electron	e25i, 2e25i	Higgs (SM, MSSM), new gauge bosons extra dimensions, SUSY, W, top
Photon	γ60i, 2γ20i	Higgs (SM, MSSM), extra dimensions, SUSY
Muon	μ20i, 2μ10	Higgs (SM, MSSM), new gauge bosons extra dimensions, SUSY, W, top
Jet	j400, 3j150, 4j100	SUSY, compositeness, resonances
Jet + Missing E_T	j60 + xE60	SUSY, leptoquarks
Tau + Missing E_T	τ30 + xE40	Extended Higgs models (e.g. MSSM), SUSY

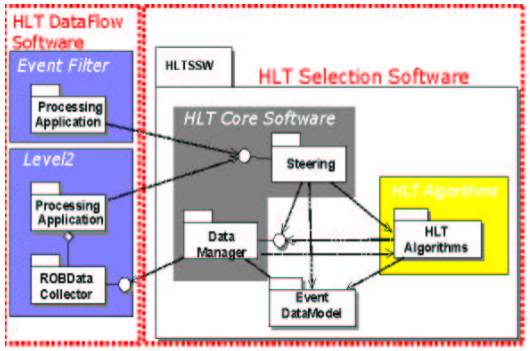

Figure 2.4: *Package diagram and external dependencies of the HLTSSW.*

needed are transferred. As in most cases un-interesting events are rejected in that early stage and in a short period of time, the RoI mechanism is a powerful way for fulfilling the HTL requirements for quick and efficient response.

2.2.2 Event selection strategy at the HLT.

The strategy for the event selection involves two main design features:

- **The use of the RoI mechanism**. Not only the selected RoIs are of major importance, but the **size** of them contributes in a large extent. For instance, the typical size of a RoI defined by LVL1 and which contains an electromagnetic cluster is (0.4×0.4) in (η, ϕ) space. But, at LVL2, where the full granularity information from the calorimeter is used, the size can be reduced to (0.2×0.2). This results in requiring and - finally processing of- smaller amount of data from the inner detector. Even at the last level (Event Filter), instead of processing the full event, the reconstruction will be seeded by the refined LVL2 RoIs. The aim here is to minimise the processing time as well as the network traffic.

- **The step-by-step signature validation**. The event processing checks at each step for the **physics signatures** in a trigger menu. Table 2.1[1] gives some examples of the selection signatures and the corresponding physics channels these cover. For instance, for a RoI that has been formed by LVL1 and containes an electromagnetic cluster, the first task for the LVL2 is, by calling the **Reconstruction** and **Hypothesis algorithms**, to check the shape of this cluster and, if that matches to that from an electron or photon, then to look for the selection signature. Usually, the selection signatures involve the existence of reconstructed tracks, specific p_T thresholds and isolation criteria. The aim here is to reject the un-interesting events at a very early stage.

2.2.3 Event Selection Software.

The HLT Event Selection Software (HLTSSW) is the structure into which all the above steps will be implemented. Fig. 2.4 gives an overview of the main components and the important external dependencies of the

[1] For example, 2e25i means that 2 isolated electrons with $p_T > 25\ GeV$ are required.

HLTSSW. We can roughly talk about four components:

- **Steering**: It controls the sequence in which the algorithms will run.
- **Data Manager**: It handles the event and all the data, which relate to the trigger. It provides each trigger level with the data needed, either from the memory (in the case of the EF) or requesting them by the ROB Data Provider (in the case of LVL2).
- **Event Data Model**: It ensures the interface between the different algorithms through common event data entities (such as a Track or Space Point).
- **HLT Algorithms**: This component includes all the different HLT Algorithms. For example, some algorithms used thoughout my studies untill now are the IDScan and SiTrack for the Pixel and SCT detectors and T2Calo for the Electromagnetic calorimeter.

2.2.4 ATHENA.

ATHENA [5] is the software framework for ATLAS. It provides common services, such as the **Transient Data Store** (TES), the **Detector Data Store**, **Message Service**, **Histogram Service** and **Job Configuration and Auditing**. The main idea is to improve the coherency of the different software domains within ATLAS, thus providing the same well-defined interfaces not only to the developers, but also to the end-users. The HLT Software runs into ATHENA, so that it ensures that all the different components keep the dependencies between them, as the individual packages are being developed. Specifically, the boundary between LVL2 and EF is now more flexible and algorithms can be developed in a more consistent way.

IDScan.

IDScan [6] is a LVL2 track reconstruction algorithm and it runs under the ATHENA environment. The major task is the track reconstrunction inside the inner detector and this is done by using the **Space Points (SPs)** from the Pixel and SCT detectors[2]. The algorithm returns the track parameters and the corresponding error matrix. It's worth saying that the online version of IDScan is designed to run several times per event and once per RoI.

In order to reduce the large amount of SP combinatories at the SCT and Pixel detectors, IDScan bases its perfomance on two main features: (1.) At the LHC, the pp interactions are expected to occur with a spread of about $\pm$**6 cm** (RMS) along the z axis, around the center of the ATLAS detector. (2.) The interesting physics events give particles with average transverse momentum higher ($p_T > 0.5\ GeV$) than the pile-up.

The design of IDScan is implemented with the following four components [7, 8]:

- **z-Finder**: It determines the z position of primary interactions (z_V)using pairs or triplets of SP from the SCT and Pixel. z_V is determined with a resolution of $\sigma_{z_V} = (180 \pm 5)\,\mu m$ and the efficiency is approximately 97%.
- **Hit Filter**: It selects "good" SPs in several different detector layers within a small solid angle. It is based on the fact that SPs of tracks coming from z_V have all the same η, while those tracks not originating from the interaction vertex have a wide spread in η. For tracks with $p_T > 2\ GeV$, the achieved efficiency is essentially 100%.
- **Group Cleaner**: Group Cleaner operates on individual groups of SPs produced by the Hit Filter. It removes any noise hits that have remained and creates the track candidates.
- **Track Fitter**: At this step, all the remaining track candidates are fitted to give all the track parameters.

[2]The Pixel detectors give a 3D measurment of the hits, while the SCTs detector elements give 2D coordinate information. In the last case, the 3D measurment comes by combining two such detector pairs which are glued together back-to-back with a small angle between them.

Chapter 3

Performance studies.

Before presenting the basic work that has been done the last seven months, it is worth mentioning that the following analysis has been done using reconstructed data (low/high luminosity) produced under the ATHENA framework with the software release 7.0.2. Although release 7.0.2 appeared to have a lot of bugs in many aspects, it gave quite representative data sets. Therefore, I will try to produce results and comments in a more qualitative rather than quantitative sense.

Unless stated clearly, the data sets refer to 5,000 single electrons events, generated with $p_T = 25\,GeV$, at low luminosity and pile-up, and with $p_T = 30\,GeV$, at high luminosity and pile-up.

3.1 IDScan.

For the IDScan, the aim was to measure and check the performance of the z-Finder and the Track-Fitter, as well.

3.1.1 z-Finder.

As mentioned earlier, the interaction point can occur of approximately ± 6 cm (RMS) along the z axis. This is demostrated in Fig. 3.1 where the z-position of the generated vertex and the vertex that z-Finder determines are shown.

The accuracy for finding the correct z-position will be given by the distribution of the difference between the reconstructed and the generated value. Fig. 3.2 gives that histogram. The gaussian fit gives $\sigma = (179.9 \pm 2.7)\,\mu m$. But in this case one should be carefull, because this distribution is the sum of gaussian distributions which have different standard deviations. And this is due to the different response that the z-finder has in the different η-regions.

To see how the z-finding resolution depends on η, we split the η range $[0, 2.5]$ into five intervals[1], and for each one we plot the difference between the recontructed and the generated value. The σ value of the followed gaussian fits on these histograms are given in Fig. 3.3. The most important thing to notice here is the fact that at both high and low luminosity, the z-position is found with the same accuracy at each $|\eta|$ region. Moreover, better accuracy is acheved for particles with generated $|\eta| \simeq 0$ (vertical to the beam axis), rather than those with large values of $|\eta|$. This is explained by the fact the low η tracks are less sensitive to small translations than high η ones, as is demostrated in Fig. 3.4.

Finally, we calculate the efficiency for finding the z-position of the vertex. For doing so, we accept and count events for which the z-vertex was found to be inside the limits $(z_{gen} \pm 1)\,mm$. Fig. 3.5 gives the efficiency for each $|\eta|$ region, as well as the overal efficiency. The efficiency is almost constant for the range up to $|\eta| \simeq 2.0$ for both luminosities. There is a significant drop at the edges of the detector due to the selected cut, while the difference in the efficiency between the two luminosities is 10%.

3.1.2 Pattern Recognition.

The z-position of the primary vertex defined by z-Finder is used next by the pattern recognition algorithms. In order to study the behaviour of the IDScan algorithm **independently**, we used the ntuples (kineZ ntuples) in which it was the **generated** z-position of the vertex that had been given as input to the pattern

[1] Further study showed that the distribution has totally symmetrical behaviour for the negative values of η, so that we treated only absolute values.

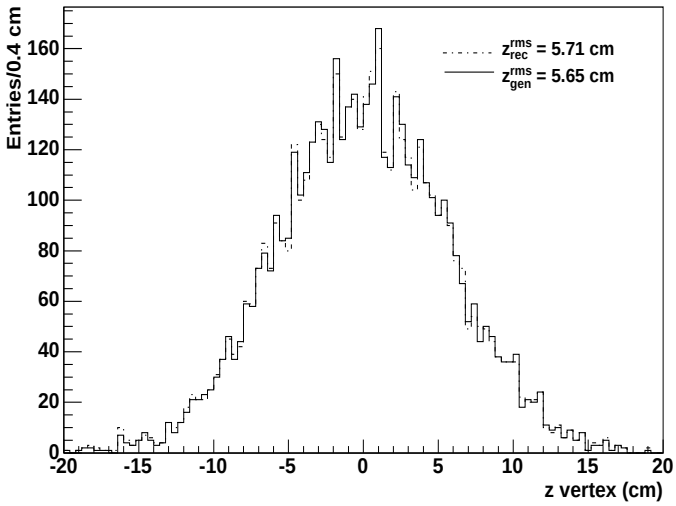

Figure 3.1: *z-coordinate of the generated (solid line) and reconstructed (dashed line) interaction vertex for low luminosity.*

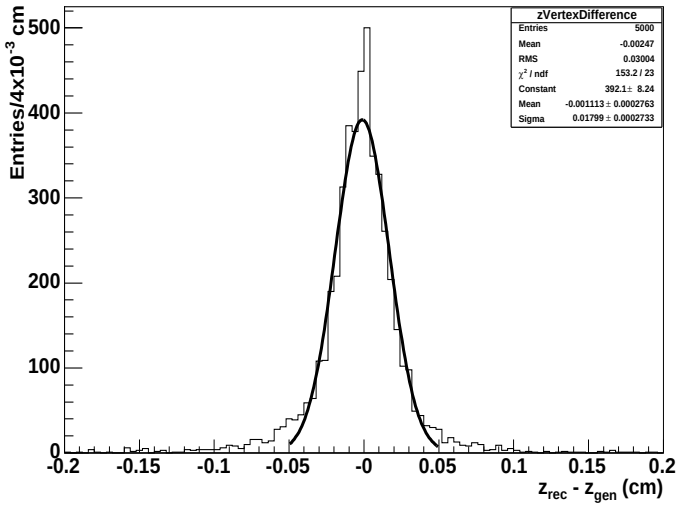

Figure 3.2: *The resolution for finding the z-coordinate . Again, the data are for low luminosity.*

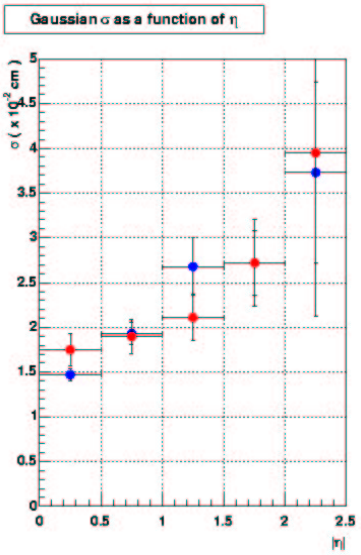

Figure 3.3: *The resolution for finding the z-coordinate as a function of $|\eta|$ for low luminosity (blue) and for high luminosity (red).*

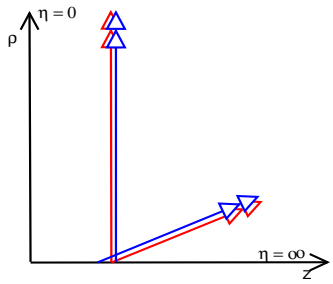

Figure 3.4: *Vertical tracks are less sensitive than inclined ones: a slight change of a vertical track affects the z position of the vertex less than a change of the same magnitude of an inclined track .*

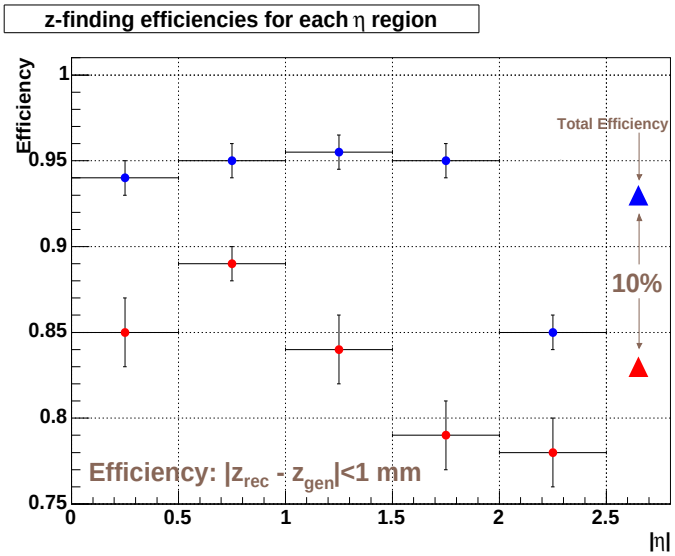

Figure 3.5: *The event efficiencies in finding the z-coordinate for low luminosity (blue) and for high luminosity (red). The efficiency is defined as $|z_{rec} - z_{gen}| < 1\,mm$. The errors were calculating using the binomial distribution.*

Table 3.1: *Track efficiencies for IDScan, xKalman and iPatRec.*

Algorithms	**Low Luminosity**	**High Luminosity**
IDScan	(89.0±0.4)%	(82.9±0.5)%
xKalman	(88.9±0.4)%	(84.0±0.5)%
iPatRec	(87.2±0.4)%	(82.2±0.5)%

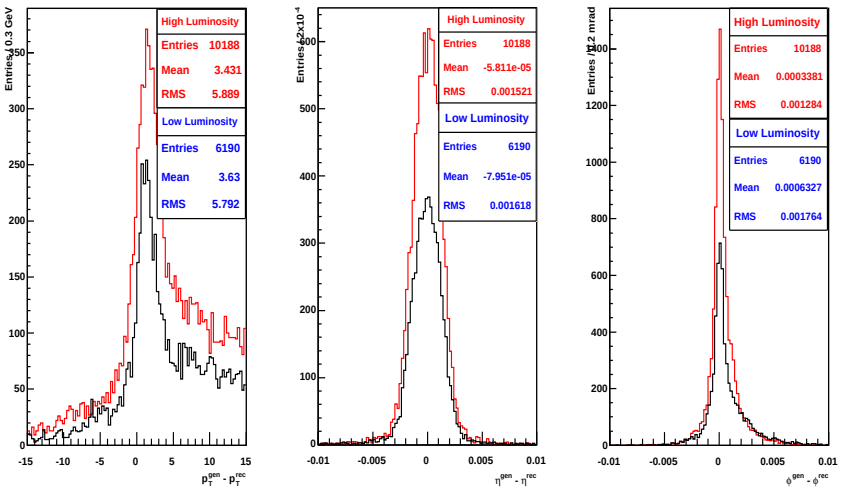

Figure 3.6: *The resolution in p_T, η, ϕ obtained by IDScan for the low (blue) and high (red) luminosity data sets.*

recognition algorithms. We will compare the efficiency performance of the IDScan algorithm (which runs on LVL2 trigger) with the xKalman and iPatRec algorithms (which run on the EF).

For the analysis, we required that each of the tracks fullfils the following conditions:

- $|p_T^{gen} - p_T^{rec}| < 15\,GeV$
- $|\eta^{gen} - \eta^{rec}| < 0.01$
- $|\phi^{gen} - \phi^{rec}| < 0.01\,rads$

With these conditions, Table 3.1 shows the total efficiency achievied by IDScan, xKalman and iPatRec for the low and high luminosity data. The efficiency obtained by IDScan is comparable to those achieved by xKalman and iPatRec. This means that we can have an efficient track acceptance at a very early stage of the triggering chain.

The distributions for the quantities $p_T^{gen} - p_T^{rec}$, $\eta^{gen} - \eta^{rec}$ and $\phi^{gen} - \phi^{rec}$ for the two luminosity values are shown in Fig. 3.6.

The above histograms include all the tracks found by IDScan and satisfy the cuts. It is obvious that for the data with pile-up, more than one tracks can be found per on generated event. Fig. 3.7 demotrates this fact. Most of the times, IDScan finds one track. But there are cases where no-track is found and some other cases where even more than four tracks are found. Recent developments of the algorithms lowered the track multiplicity down to 1: the generated track.

Finally, it is of interest to know the track efficiency of IDScan for each $|\eta|$ region. Therefore we look at the numbers of the events which have at least one track found by IDScan and which satisfies the above conditions over the total number of events which have tracks, in different $|\eta|$ regions. For the two luminosities, the results are given in Fig. 3.8. For both luminosities, the IDScan track efficiency is constant at the region $0 \leq |\eta| < 1.5$, but it falls at the edges. Again, recent developments on the tracking fitting algorithms have managed to keep the efficiency constant all over the detector.

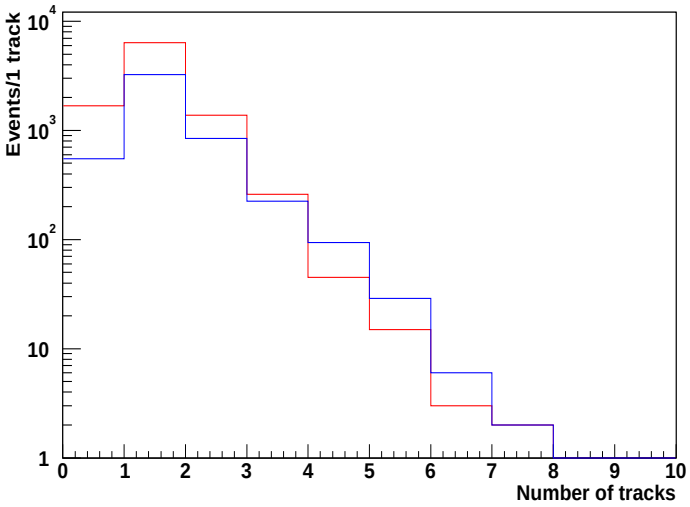

Figure 3.7: *The track multiplicity found by IDScan for the low (blue) and high (red) luminosity data sets.*

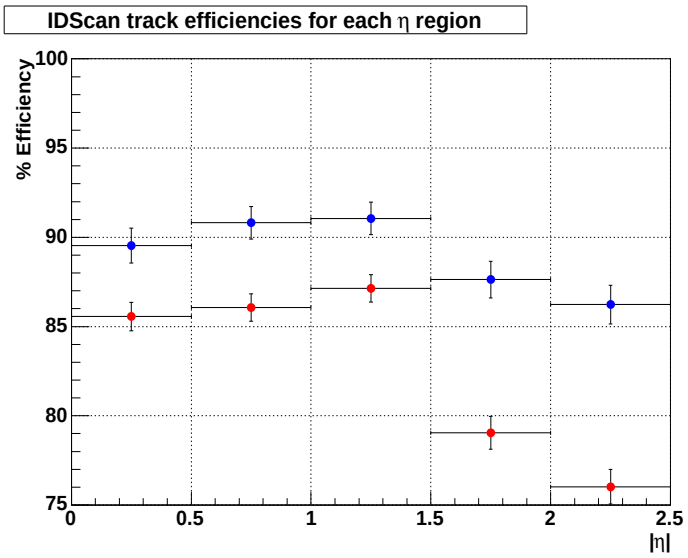

Figure 3.8: *The track efficiency for each eta region for the low (blue) and high (red) luminosity data sets.*

Table 3.2: *Efficiencies (with respect to LVL1) and rates for low luminosity single electron events ($p_T = 25\,GeV$). The figures for the LVL2ID refer to IDScan track algorithm.*

Trigger Level	% efficiency	Rates
LVL1	100	7.9 kHz
LVL2 Calo	95.7	1.9 kHz
LVL2 ID	88.4	359.1 Hz
LVL2IDCalo	86.3	136.1 Hz
EFCalo	84.8	92.3 Hz
EFID	80.0	64.1 Hz
EFIDCalo	73.4	31.3 Hz

3.2 E/gamma vertical slice.

The aim here is to determine the selection efficiency and the rates for each trigger level. By this way, we can check and improve our trigger/selection and recostruction algorithms, making them more stable, robust and fast, so that they can face the real conditions of LHC.

As mentioned before, for each interesting physics channel, there are one or more signatures that we expect to see. For the low mass Higgs, signatures involving electrons or photons are of major importance (see Section 4.2) and the whole chain which includes the reconstruction and hypothesis algorithms for making a final decision on these particles is called e/γ vertical slice. During this selection process the initial event rate of 40 MHz has to be reduced to a rate of about 30 Hz after EF, while the electron selection efficiency should be kept around 80% with respect to LVL1.

Based on a priliminary version of the framework [9], I modified to code in order to make it more flexible and easy to use. A lot of changes have been implemented [10], the most important of which has to do with the switching between the different data sets produced in each release. Comparisons with earlier versions, and thus bugs-finding, can be done now more easily and quickly. During this section, the efficiencies and rates were calculated using the same software release as that which was used for writting the latest version of HLT TDR. Therefore, a variety of data sets, for signal and background as well, is available.

For single electron events with $p_T = 25\,GeV$ at low luminosity as event signal, Table 3.2 gives the efficiencies and the rates achieved for each trigger level.

Due to the fact that there is going to be only 1 interesting event per 10^6 background events (mainly jets), the rates were calculated using approximately 175,000 fully simulated dijet event samples as backgound at low luminosity with $E_T^{jet} > 17\,GeV$. The rate is calculated using the formula:

$$Rate = \sigma \times L \times E \tag{3.1}$$

where $\sigma = 1.5\,mb$ is the cross section for the QCD process $pp \to jj$ with $E_T^{jet} > 17\,GeV$,[2] $L = 2 \times 10^{33}\,cm^{-2}s^{-1}$ is the low luminosity value and

$$E = \frac{Accepted\,Events}{Total\,Events} \tag{3.2}$$

is the efficiency at each level.[3]

In addition, changing the E_T (i.e. the transverse energy deposited at the calorimeter cell) threshold, one can see the impact on LVL2 and EF efficiencies. For 5,000 simulated $W \to e\nu_e$ events, the results are shown in Fig. 3.9. From the graph, we can determine the optimal value of E_T. A safe value for that is chosen to be 22.5 GeV.

3.3 RoI size.

In this section we are interested in determing the size of the RoI that should be used by the LVL2 tracking algorithms. This is important because it can reduce the data requesting and processing time, as well as the number of the SP combinatories inside the RoI. Although the study is in a very preliminary stage, it is worth mentioning its main methology.

[2]For the high luminosity and $E_T^{jet} > 25\,GeV$, the cross section becomes $\sigma = 0.358\,mb$.

[3]In the data sets used, eq. (3.1) should be divided by a factor of 11 to count for several cuts at particle level.

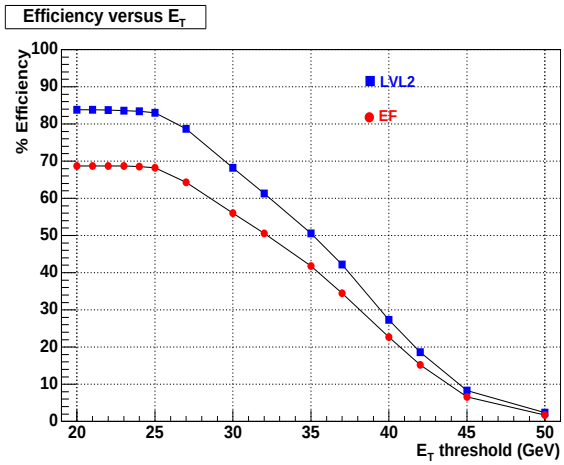

Figure 3.9: *e^- selection efficiency for $W \to e\nu_e$ low luminosity samples as a function of the E_T threshold for LVL2 and EF.*

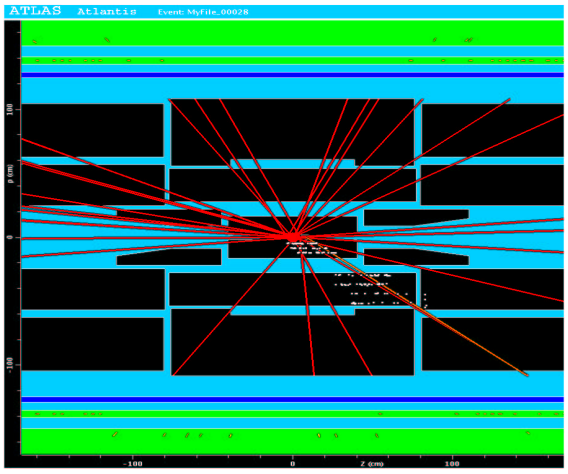

Figure 3.10: *A single electron event in high luminosity as made by the ATLANTIS event display software. Only the SPs (white markers) inside the RoI are drawn and the track found by IDScan is given in orange.*

Fig. 3.10 gives an event display made using ATLANTIS and shows the SPs inside the RoI. The current performance for constructing the RoI, inside which IDScan takes SPs and looks for tracks, is based on the following scheme: starting from the η, ϕ values given by LVL1Calo and taking into account the uncertainty in the z-position of the vertex, IDScan defines an area with size $\Delta\eta \times \Delta\phi = 0.2 \times 0.2$, (Fig. 3.11 red area). But, when we take into account the full granularity information from the calorimeter and combine it with that of the vertex then the size of the area changes (Fig. 3.11 blue area).

The size of the area depends on how well the following are known: (i) the z position of the vertex and (ii) the η, ϕ of the track, determined by the calorimeter.

The z position of the vertex can be determined with and accuracy of 180 μm, keeping in mind the fact that the bunch crossing occurs in a space of $\pm 20\, cm$ around z = 0 (see Section 3.1.1).

The phi resolution (Fig. 3.12) is almost 3 $mrad$.

Due to the fact that the eta value of the cluster is calculated with respect to $z = 0$, the eta resolution depends strongly on the z position of the vertex. Fig 3.13 shows how the resolution in η changes if we require tracks that were generated inside the window $z_V = \pm 2\ mm$. In addition, Fig. 3.14 gives the eta resolution as a funtion of the generated z, η and ϕ. As there no dependence on the azimouthal angle because of the cylidrical symmetry, there is a dependence on the z position of the vertex and on the polar angle. Tracks which were born away from $z = 0$ or tracks which are vertical to the beam axis give worse resolution in the calorimeter, in terms of η.

Instead, in order to avoid that dependence, we can speak in terms of the z resolution of the EM calorimeter at the barrel and of the ρ resolution at the endcap region. This is given in Fig. 3.15. The z coordinate of

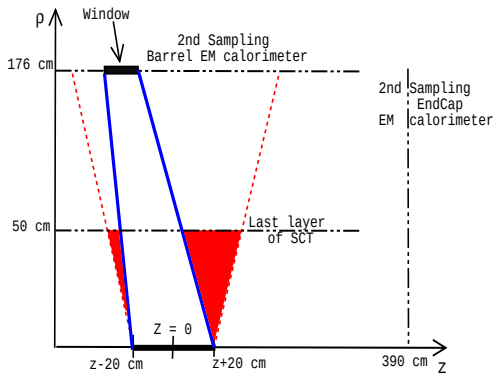

Figure 3.11: *The RoI as it is formed by the inner detector only (red area) and using the information from the EM clusters (blue).*

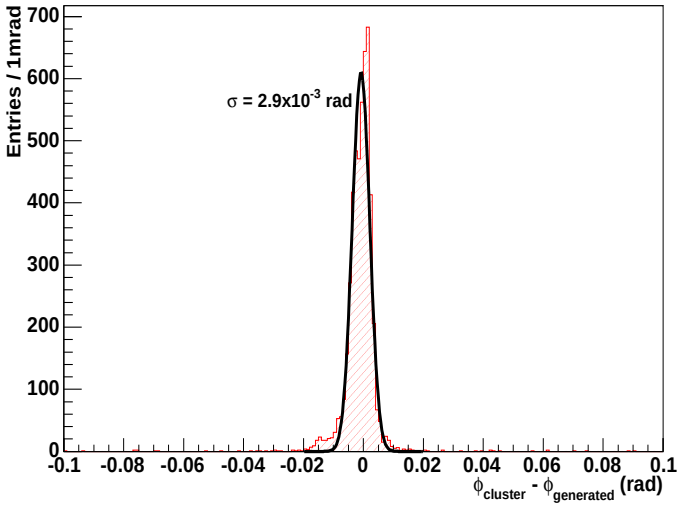

Figure 3.12: *The ϕ resolution given by the EM calorimeter. The distribution is after extrapolating the ϕ value of the cluster back to the vertex.*

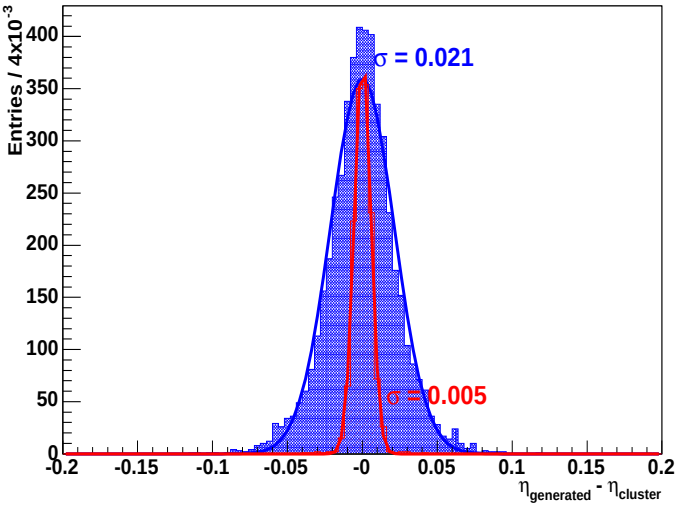

Figure 3.13: *The η resolution given by the EM calorimeter. The red distribution corresponds to tracks that were generated ± 2 mm away from $z = 0$ only. The change is of an order of magnitude.*

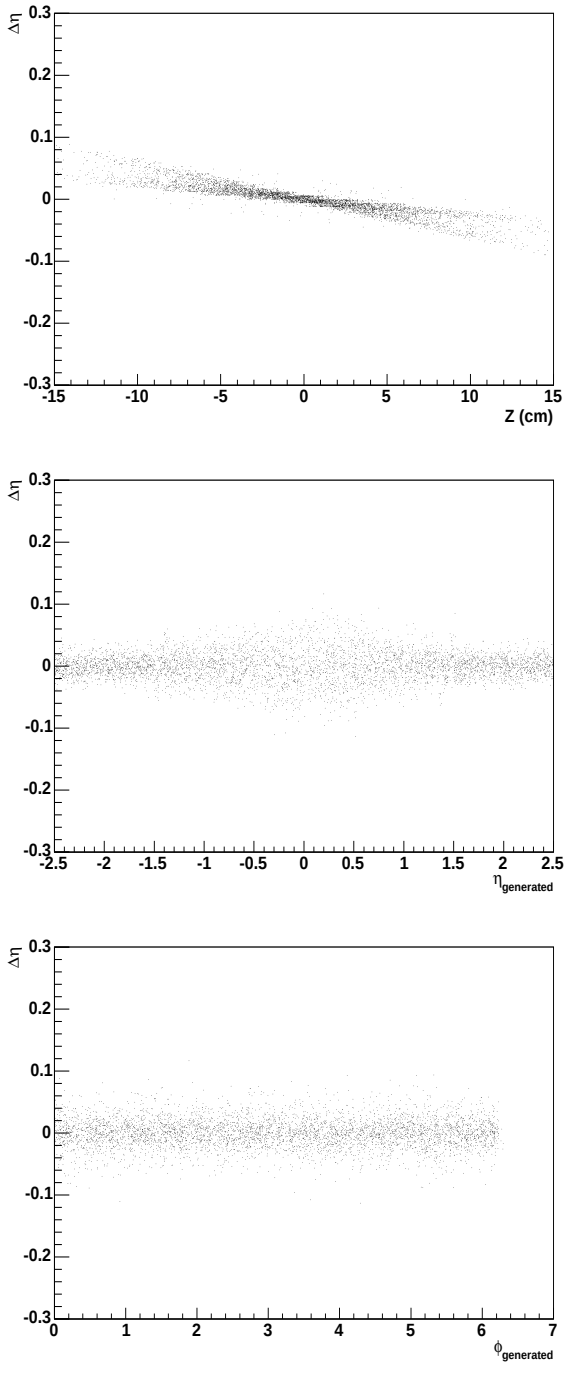

Figure 3.14: *The η resolution given by the EM calorimeter as a function of the generated z, η and ϕ.*

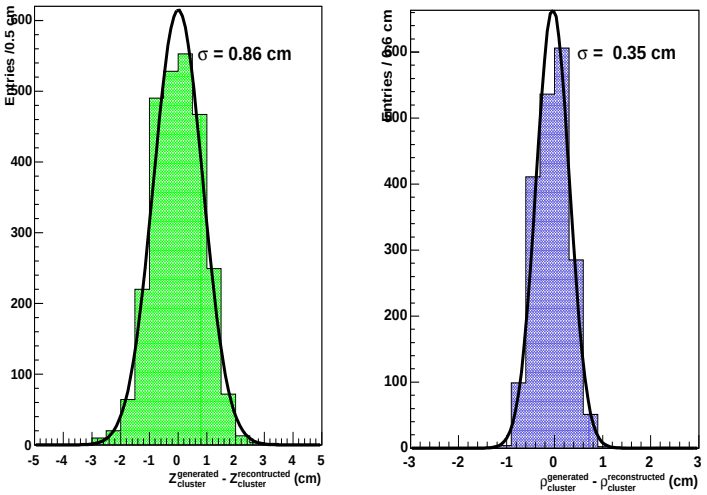

Figure 3.15: *The z resolution given by the Barrel EM calorimeter (left) and the ρ resolution given by the EndCap EM calorimeter (right).*

the intersection of the track with the barrel EM calorimeter can be determined with a resolution of about 9 mm and with 4 mm at the endcap. The next step is to change the RoI size used at the very begining of IDScan and see the effects caused by these changes.

Chapter 4

Future plans

4.1 Performance studies.

In the very near future, my performance studies will mainly be focused on:

1. **E/gamma selection algorithm**. The e/gamma framework is still under improvement, as far as its functionality is concerned. There is a big effort put on that in order to reach a stable and robust version, while at the same time the efficiencies must be validated at each release. The next step is to check its physics aspects. That means that I intend to go into the physics details of the selection codes, studing the numerical values of the cuts, checking their efficiency and in general try to fix or add features from the selection design at each trigger level. While the whole package of the Trigger Analysis is constantly being impoved, the e/gamma framework will be a way to check each data production and to point out any bugs or what it's missing from the individual codes.

2. **IDScan**. The size of the selected RoIs has to be optimized. This involves further studies of the code and modifications in order to implement the changes of the RoI size and see how these affect the overall performance. I hope that this will be a subject for a future ATLAS note.

3. **2004 Test Beam**: At the next combined test beam held at CERN, I will have the chance to perform timing and triggering tests with the real data from the beam. The Trigger Algorithms will run in real environment and with the test bed set up by the UCL group, I will study the timing performace of the HLT chain.

4.2 Physics studies.

Although I haven't decided yet the specific process that I shall be studying, my interest will be focused on the low mass ($m_H < 150\,GeV$) Standard Model Higgs boson.

Fig. 4.1 gives the Feynman diagrams for the four processes for the Higgs production. The production is dominated by the gluon-gluon fusion with a cross section during the high luminosity phase of LHC of about 30 pb. The second largest cross section comes from the fusion of vector bosons radiated by initial-state quarks.

Although, the direct production $gg \to H$ cannot be triggered with significant efficiency because of the huge QCD background, the production of the Higgs boson through the quark-quark channel (WW/ZZ fusion) is the clearest one and can be spotted because it is accompanied by two jets in the forward regions of the detector, originated from the initial quarks that emit the vector bosons. Therefore, jet tagging in the forward region with a veto of jet activity in the central region can be used in order to trigger that channel.

Fig. 4.2 gives the main decay channels as a function of the Higgs mass. Higgs decays into relatively heavy quarks or bosons, like $b\bar{b}, t\bar{t}, WW, ZZ$, because the coupling constant with the decay products is analogous to their mass. For the low mass Higgs case, there are two major decay channels:

4.2.1 $H \to \gamma\gamma$

It is a promising channel for Higgs searches in the mass range up to 150 GeV. But it is a very rare decay mode, because the $H\gamma\gamma$ coupling is forbidden at the tree level and therefore the decay occurs only at higher order

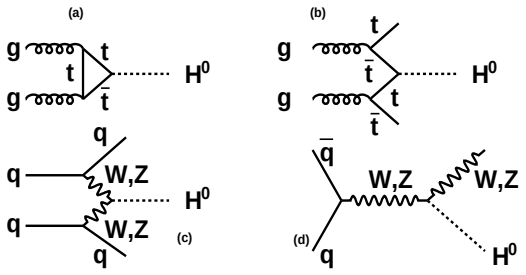

Figure 4.1: *Feynman diagrams for the Higgs production processes at the Standard Model. (a) gluon-gluon fusion (b)associated $t\bar{t}$ production (c) WW and ZZ fusion (d) W/Z Higgs-strahlung radiation.*

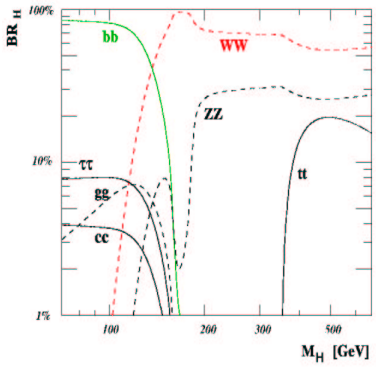

Figure 4.2: *Branching ratios for the Higgs decay channels as a function of its mass. From [11].*

through a W loop (Fig. 4.3(a)). For triggering this channel, we require two high-p_T photons ($p_T \sim 50\,GeV$) with invariant mass compatible with the Higgs mass.

The main two large background channels are: (i) the irreducible (which gives exactly the same final state as the signal) includes the $\gamma\gamma$ production by gluons or quarks as given in Fig. 4.3(b,c). Fig. 4.4 shows the expected $H \to \gamma\gamma$ signal on top of that continuum background (ii) the reducible γj or jj production, where one or both jets are misidentified as photons. This is the case when the jets include soft particles or hard π^os which give two photons, very close to each other. In the latter case, the two photons appear as one inside the calorimeter, thus giving a fake signal. Fig. 4.5 shows the shower profile in the strips at the first longitudinal compartment of the EM calorimeter. The segmentations of theses strips (4 mm pitch in the η direction) allows the seperation between these two γ's.

As shown in Table 4.1, Higgs can be detected in the ATLAS detector by this channel with a significance more than 5σ.

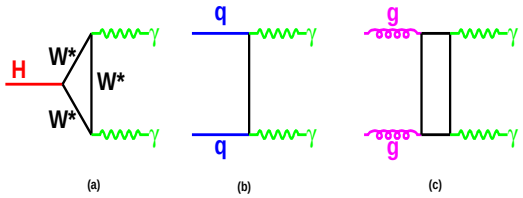

Figure 4.3: *Feynman diagrams for (a) Higgs decays into photons through a W loop (b, c) $\gamma\gamma$ production through the Born and box processes.*

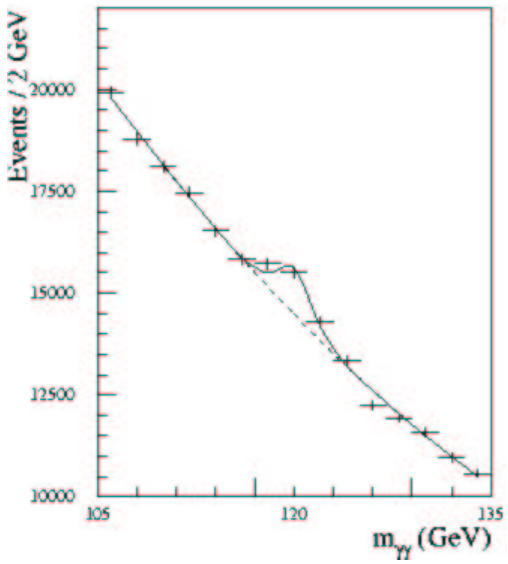

Figure 4.4: *Expected $H \to \gamma\gamma$ signal for $m_H = 120$ GeV and for an integrated luminosity of 100 fb^{-1}. The signal is shown on top of the irreducible background. From [2].*

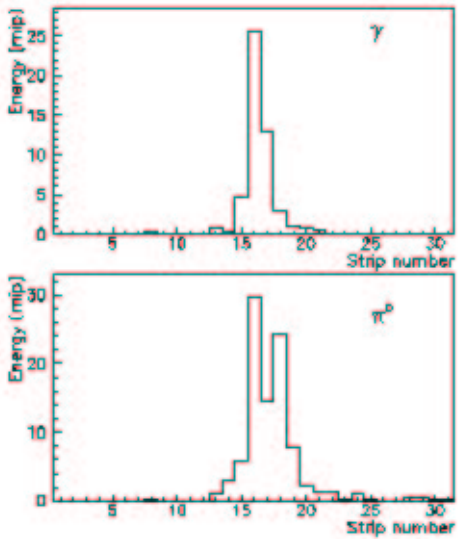

Figure 4.5: *Shower lateral profile in the η strips of the ATLAS EM calorimeter from a GEAN-based simulation of single photon (up) and of $\pi^o \to \gamma\gamma$ events (down). From [2].*

Table 4.1: *Observability of the $H \to \gamma\gamma$ decay channel for $120 < m_H < 150$ GeV. The numbers are given for $L = 100\ fb^{-1}$. From [2].*

m_H **(GeV)**	**120**	**130**	**140**	**150**
Signal Events (S)	1190	1110	915	617
Background Events (B)	29000	24700	20600	16900
$S/\sqrt{B}$ ratio	6.5	6.5	5.8	4.3

Table 4.2: *Expected ttH signal and background rates for* $m_H = 120\ GeV$ *for integrated luminosity of* $L = 30\ fb^{-1}$ *and* $L = 100\ fb^{-1}$. *From [2].*

	$L = 30\ fb^{-1}$	$L = 100\ fb^{-1}$
Signal Events (S)	40	62
$t\bar{t}Z$	2	5
$W + 4j$	5	10
$t\bar{t} + 2j$	120	242
Background Events (B)	127	257
S/B **ratio**	0.32	0.24
$S/\sqrt{B}$ **ratio**	3.6	3.9
$S_{H\to b\bar{b}}/S_{total}$ **ratio**	0.59	0.50

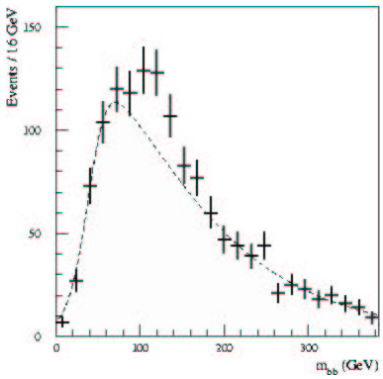

Figure 4.6: *Invariant mass distribution,* $m_{b\bar{b}}$ *, of b-tagged jets in fully reconstructed* $t\bar{t}H$ *signal events with* $m_H = 120\ GeV$. *The dashed line is the summed background. From [2].*

4.2.2 $H \to b\bar{b}$

This channel is the dominant one for low mass Higgs giving a branching ratio of about 90% of the time. Since the direct production, $gg \to H$ with $H \to b\bar{b}$ can not be efficiently triggered due the QCD background, the associated $t\bar{t}$ production is the dominant process to observe that channel. The semileptonic decays of the W boson ($W \to \ell\nu_\ell$) coming from the decay of one of the top quarks ($t \to Wb$) provide an isolated high-p_T lepton for triggering. In addition, the requiriment of this high-p_T lepton provides a large rejection against background from QCD jet production. Then, the Higgs-boson can be reconstructed from the invariant mass of the four b-tagged jets.

Here, the background can be: (i) the irreducible background, consisting of the resonant $t\bar{t}Z$ with the $Z \to b\bar{b}$ decay and of the $t\bar{t}b\bar{b}$ production (ii) the reducible background, which contains jets misidentified as b-jets, such as $t\bar{t}jj$, $Wjjjj$, $Wjbb$ etc. The better the b-tagging performance achieved, the less this background contributes.

Table 4.2 gives the expected signal and background rates for this channel and for $m_H = 120\ GeV$. The $t\bar{t}jj$ background is the dominant one. Finally, Fig. 4.6 gives the invariant mass distribution of tagged b-jets pairs for a Higgs mass of $m_H = 120\ GeV$.

In general, my task will include the study of the full production line: (i) Event generator (ii) Event simulation and (iii) Event reconstruction. I will try to investigate physics processes and properties that will be an important contribution to the Collaboration and throughout my analysis, I will try to introduce flexible and general codes, which will be easily used by others.

Bibliography

[1] http://lhc-new-homepage.web.cern.ch/lhc-new-homepage/DashBoard/index.asp

[2] ATLAS Collaboration: **"Detector and Physics Performance".** Technical Design Report (CERN/LHCC/99-14 ATLAS TDR 14).

[3] F. Gianotti: "**Collider Physics: LHC"**. Lectures given at the European School of High-Energy Physics, Casta Papiernicka, September 1999. ATLAS Internal note CONF-2000-001, April 200.

[4] ATLAS **"High-Level Trigger Data Acquistion and Controls**". Technical Design Report (CERN/LHCC/2003-022).

[5] http://atlas.web.cern.ch/Atlas/GROUPS/SOFTWARE/OO/architecture/index.html

[6] N. Konstantinidis, H. Drevermann: **"Fast tracking in hadron collider experiments"**. ACAT2000 Conference Proceedings, page 130, October 2000.

[7] N. Konstantinidis, H. Drevermann: **"Algorithms to select space points of tracks from single primary interactions in ATLAS"**. (ATL-COM-DAQ-2003-040)

[8] N. Konstantinidis, H. Drevermann:**"Determination of the z position of primary interactions in ATLAS prior to track reconstruction"**. (ATL-DAQ-2002-014)

[9] See M.Diaz-Gomez, E. Moyse, V. Perez-Reale, C. Padilla, A. Wildauer: **"The e/γ Analysis Framework: Efficiency and rate studies for the ATLAS High-Level Trigger TDR and beyond"** at http://wildauer.home.cern.ch/wildauer/egamma/index.html

[10] For detailed records and features see:
http://atlas-sw.cern.ch/cgi-bin/viewcvs-atlas.cgi/offline/Trigger/TrigAnalysis/TrigNtEgamma/
and:
http://www.hep.ucl.ac.uk/~sstef/EGammaAnalysis.html

[11] Niels Meyer, Klaus Desch: **"The Higgs Bosons Width through WW fusion at TESLA"**. ECFA-DESY Workshop on Linear Collidersss, Padova, May 5th - 8th 2000.